

# Bayesian inferences on covariant density functionals from multimessenger astrophysical data: The influences of parametrizations of density dependent couplings

Guo-Jun Wei<sup>a,b,c</sup>, Jia-Jie Li<sup>c</sup>, Armen Sedrakian<sup>d,e</sup>, Yong-Jia Wang<sup>b</sup>, Qing-Feng Li<sup>b,f</sup>, Fu-Hu Liu<sup>a</sup>

<sup>a</sup>*Institute of Theoretical Physics, Shanxi University, Taiyuan 030006, China*

<sup>b</sup>*School of Science, Huzhou University, Huzhou 313000, China*

<sup>c</sup>*School of Physical Science and Technology, Southwest University, Chongqing 400715, China*

<sup>d</sup>*Frankfurt Institute for Advanced Studies, D-60438 Frankfurt am Main, Germany*

<sup>e</sup>*Institute of Theoretical Physics, University of Wrocław, 50-204 Wrocław, Poland*

<sup>f</sup>*China Institute of Atomic Energy, Beijing 102413, China*

## Abstract

Covariant density functionals have been successfully applied to the description of finite nuclei and dense nuclear matter. These functionals are often constructed by introducing density dependence into the nucleon–meson couplings, typically through functions that depend only on the vector, i.e., proper baryon density. In this work, we employ a Bayesian framework to investigate how different parametrizations, characterized by distinct functional forms and by their dependencies on vector and scalar densities, affect the properties of dense matter and compact stars. Our analysis demonstrates that although all considered parametrizations yield broadly comparable inferences, the differences in the equation of state and the symmetry energy remain significant at suprasaturation densities, reflecting the sensitivity to the chosen functional form of the density dependence. We find that allowing the nuclear saturation properties in the isoscalar channel, including the skewness coefficient  $Q_{\text{sat}}$ , to be freely adjusted provides adequate flexibility for the current modeling of nuclear and neutron star matter. In contrast, the isovector channel requires further refinement, with freedom extended at least up to the curvature coefficient  $K_{\text{sym}}$  to capture variations in the symmetry energy and particle composition at high densities. This work advances prior studies by implementing a rational-function parametrization of the density dependence, informed and constrained by multimessenger astrophysical observations.

**Keywords:** Equation of state, Compact stars, Covariant density functional, Bayesian inference

## 1. Introduction

Understanding the behavior of dense hadronic matter is one of the central challenges in nuclear physics and astrophysics. The equation of state (EOS) of nuclear matter serves as a crucial bridge between the microscopic nucleon dynamics governed by nucleon–nucleon interactions and the macroscopic properties of compact stars (CSs), which are among the most extreme objects in the universe. With densities up to 5–10 times higher than those found in ordinary nuclei, CSs offer a unique setting for studying the EOS of dense matter under conditions that are impossible to achieve in terrestrial laboratories; for reviews of the EOS of CSs, see Refs. [1, 2].

Recent advances in astrophysical observations and terrestrial experiments have greatly enhanced our capacity to probe the nuclear EOS. These developments include: (a) constraints on CS deformability derived by LIGO–Virgo collaboration from gravitational waves emitted during binary neutron star mergers [3–7]; (b) radius measurements of several CSs obtained by the NICER X-ray observatory [8–16]; and (c) measurements by

the PREX and CREX experiments [17–20] of the neutron skin of nuclei in parity-violating electron scattering experiments that allowed the extraction of the slope of the symmetry energy. Additional valuable constraints are provided by ab initio studies based on nucleon–nucleon potentials derived from the chiral effective field theory ( $\chi$ EFT) framework. These include predictions for neutron matter using realistic two- and three-nucleon interactions, which remain valid within the  $\chi$ EFT setup up to approximately 1.5–2 times the saturation density [21–24]. Similarly, ab initio calculations can be performed in the perturbative quantum chromodynamics (pQCD) regime at extremely high densities, around 40 times the saturation density. Such calculations provide an effective boundary condition for models that are extrapolated to the high-density regime [25–27].

The EOS of the dense hadronic phase in CSs can be constructed using a variety of approaches, including density functional methods [28–34], meta-models [35–38], and model-agnostic descriptions [39–47]. Among these, covariant density functional (CDF) theory [48, 49]—rooted in the quantum field theory of hadronic matter—provides a unified framework capable of addressing the full range of nuclear data, from the nuclide chart to the physics of CSs [1, 2, 50]. The class of CDF models are based on relativistic Lagrangians describing nucleons – constituents of dense hadronic matter – as interacting via me-

Email addresses: jiajieli@swu.edu.cn (Jia-Jie Li), sedrakian@fias.uni-frankfurt.de (Armen Sedrakian), wangyj@zjhu.edu.cn (Yong-Jia Wang), liqf@zjhu.edu.cn (Qing-Feng Li)

son exchange. They maintain key relativistic features, such as Lorentz covariance, the Dirac structure of the self-energies, etc. In recent years, the increasing availability of theoretical, observational, and experimental constraints has enabled the development of CDF-based multiphysics Bayesian inference frameworks, which have emerged as a powerful tool for deriving and systematically refining constraints on the CS and nuclear matter EOS [51–64].

The CDF models are generally categorized into two classes: (a) those with constant meson–nucleon couplings that incorporate nonlinear meson self-interactions and/or cross-interaction terms into the effective Lagrangian, and (b) those that retain only linear couplings but introduce explicit density dependences in the couplings to account for medium modifications of the meson–nucleon vertices; for review see Refs. [1, 2, 50]. While both types of CDF models show convergent behavior at low densities, where physics is constrained by well-understood properties of nuclear matter under laboratory conditions, their predictions regarding the behavior of matter under extreme conditions – such as at densities far beyond saturation – rely heavily on the underlying assumptions for the nonlinear terms in the Lagrangian or the functional dependence of the meson–nucleon couplings.

In the present work, we perform a comprehensive Bayesian analysis that systematically compares CDF models of the second type (density-dependent CDFs) featuring different choices of the density – either scalar or vector – entering the prescribed functional dependence, while employing identical multiphysics constraints and a consistent computational framework. It has long been recognized that CDF models operate with two types of densities: the vector density and the scalar density [65]. In most models, the meson–nucleon couplings depend on the vector density with specific functional forms characterizing this dependence [29, 30, 66–73]. Only recently has a dependence on the scalar density, or a mixture of the two densities, been explored in the description of finite nuclei [71] and CS matter [72, 74] using specific sets of parametrizations.

Regarding the functional form of the density dependence, in the widely adopted density-dependent (DD) CDF models, particularly the DD-ME version [66, 69], the isoscalar meson–nucleon couplings are described by two rational functions with constraints imposed among their parameters, while an exponential function is used for the isovector meson. This formulation results in a model with seven free parameters, enabling adjustment of nuclear matter saturation properties up to the skewness coefficient  $Q_{\text{sat}}$  for symmetric nuclear matter and up to the slope coefficient  $L_{\text{sym}}$  for the symmetry energy of isospin asymmetrical nuclear matter [34, 75, 76]. In the present work, we consider extensions and generalizations of the density-dependent functional forms of the meson–nucleon couplings to allow greater flexibility, with the goal of probing the influence of higher-order nuclear characteristic coefficients at saturation, defined through the familiar Taylor expansion of the energy density of nuclear matter around the saturation density and isospin symmetrical limits.

## 2. Density-dependant CDF theory

We now briefly review several key aspects of the CDF approach with density-dependent couplings, putting the emphasis on the modifications implemented in the functional forms of the density dependence.

### 2.1. Effective Lagrangian and nucleon self-energy

The Lagrangian of stellar matter with nucleonic degrees of freedom is given by the sum of the nucleonic, mesonic, and leptonic free Lagrangians, which can be found in Refs. [1, 2, 50], and the interaction Lagrangian, which reads

$$\mathcal{L}_{\text{int}} = \sum_{n=n,p} \bar{\psi}_n (g_\sigma \sigma - g_\omega \gamma_\mu \omega^\mu - g_\rho \gamma_\mu \boldsymbol{\tau}_n \cdot \boldsymbol{\rho}^\mu) \psi_n. \quad (1)$$

where  $\psi_n$  stands for the nucleonic [neutron ( $n$ ) and proton ( $p$ )] fields,  $\boldsymbol{\tau}_n$  is the isospin vector,  $g_m$  ( $m = \sigma, \omega$  and  $\rho$ ) are the meson-nucleon coupling strengths. The Lagrangian (1) comprises the minimal set of interaction vertices necessary for a quantitative description of nuclear phenomena. The Dirac Hamiltonian for nucleons is given by

$$\mathcal{H} = \sum_{n=n,p} [\boldsymbol{\alpha} \cdot \mathbf{p} + \beta(m_n - \Sigma_S) + \Sigma_V^n], \quad (2)$$

where  $\boldsymbol{\alpha}$  and  $\beta$  are the well-known Dirac matrices, the first coupling the upper and lower components of the Dirac spinor, and the second, distinguishing between positive- and negative-energy states. The  $\Sigma_S$  and  $\Sigma_V^n$  are the scalar and vector self-energies of an in-medium nucleon, and can be expressed as

$$\Sigma_S = g_\sigma \sigma + \Sigma_R^S, \quad \Sigma_V^n = g_\omega \omega + g_\rho \rho \tau_{3n} + \Sigma_R^V. \quad (3)$$

The rearrangement terms  $\Sigma_R^{S(V)}$  arise from the dependence of the couplings on the scalar or vector densities, and are mandatory for maintaining the thermodynamic consistency of the model [65, 66]. Note that in Eq. (3) only the time-like components of the vector meson fields contribute, as required by rotational invariance and charge conservation.

In the mean-field approximation, the meson fields are replaced by their respective expectation values,

$$\bar{\sigma} = \frac{1}{m_\sigma^2} g_\sigma n_s, \quad \bar{\omega} = \frac{1}{m_\omega^2} g_\omega n_v, \quad \bar{\rho} = \frac{1}{m_\rho^2} g_\rho n_{v3}, \quad (4)$$

where the scalar and vector densities at zero temperature are given by

$$n_s \equiv \langle \bar{\psi} \psi \rangle = \sum_{n=n,p} \frac{1}{\pi^2} \int_0^{k_{F_n}} \frac{m_{D,n}^*}{\sqrt{k^2 + m_{D,n}^{*2}}} k^2 dk, \quad (5a)$$

$$n_v \equiv \langle \bar{\psi} \boldsymbol{\gamma} \boldsymbol{\psi} \rangle = \sum_{n=n,p} \frac{1}{\pi^2} \int_0^{k_{F_n}} k^2 dk = \sum_{n=n,p} \frac{1}{3\pi^2} k_{F_n}^3, \quad (5b)$$

with  $k_{F_n}$  being the neutron ( $n$ ) or proton ( $p$ ) Fermi momentum, and  $m_{D,n}^* = m_n - \Sigma_S$  the Dirac effective mass. The difference between the scalar and vector (baryon) densities arises from the

additional factor  $m_{D,n}^*/(k^2 + m_{D,n}^{*2})^{1/2}$  in the scalar-density integrand. This term reflects Lorentz contraction, which suppresses the scalar contribution of highly relativistic nucleons in the limit  $k \gg m_{D,n}^*$ . Clearly, the scalar density is always smaller than the vector density.

In numerical calculations, we assume  $m_n = m_p$  fixed at the average bare mass of a nucleon; then, the nucleon Dirac mass is independent of the isospin. For lepton masses we take their vacuum values, whereas for the mesons we adopt masses close to their vacuum values, as given explicitly in Refs. [61, 62]. The EOS and the composition of stellar matter are then obtained by combining the above relations with global charge neutrality and  $\beta$ -equilibrium conditions, which determine the relations among the chemical potentials of the various particle species [77].

## 2.2. Parametrizations of density-dependent couplings

The density-dependent couplings  $g_m$  are the central quantities that determine the quality of a CDF model. They are usually written in the form:

$$g_m(n) = g_m(n_{\text{ref}}) f_m(r), \quad (6)$$

with constant values  $g_m(n_{\text{ref}})$  at a reference density  $n_{\text{ref}}$  and in principle arbitrary functions  $f_m(r)$  that depend on the ratio  $r = n/n_{\text{ref}}$ . Within the coupling vertices adopted in Lagrangian (1) the (total) number density  $n$  can be the vector or scalar density, and  $n_{\text{ref}}$ , frequently, is the corresponding value at saturation density  $n_{\text{sat}}$ .

It is common to adopt for  $f(r)$  either a rational (R) function [66, 69]

$$f(r) = a \frac{1 + b(r+d)^2}{1 + c(r+d)^2}, \quad (7)$$

or an exponential (E) form,

$$f(r) = \exp[-a(r-1)]. \quad (8)$$

These functions were originally introduced to reproduce results from Dirac–Brueckner–Hartree–Fock calculations [78], with all couplings required to decrease with increasing density. A notable feature of the functional forms in Eqs. (7) and (8) is their well-behaved asymptotic behavior as  $r \rightarrow \infty$ , where they approach either a constant value (specifically  $ab/c$ ) in the rational case, or vanish in the exponential case.

In the widely used DD-ME version [66, 69, 72], the couplings  $g_m$  depend on the vector (V) density  $n_v$ . For the isoscalar mesons  $\sigma$  and  $\omega$ , the rational function (7) is employed, but with additional constraints. Specifically, for each meson, the function is normalized at saturation  $r = 1$  and its curvature vanishes at  $r = 0$  [66, 69],

$$f(1) = 1, \quad f''(0) = 0, \quad (9)$$

and the two mesons share the constraint

$$f''_{\sigma}(1) = f''_{\omega}(1). \quad (10)$$

These restrictions reduce the number of independent parameters to three, i.e.,  $a_{\sigma}$ ,  $d_{\sigma}$ , and  $d_{\omega}$  [34, 61].

Table 1: The CDF models that are explored in this work. For each model, we specify the type of density dependence, the functional form and condition applied to the isoscalar  $\sigma$  and  $\omega$  mesons and the isovector  $\rho$  meson, and the total number of independent parameters of the model in the last column.

Model	Type	$f_{\sigma}, f_{\omega}$	$f_{\rho}$	No.
VRE	V	R, (9) and (10)	E	7
MRE	M	R, (9) and (10)	E	7
MRE2	M	R, (9)	E	8
VRR	V	R, (9) and (10)	R, (11)	7
VRR2	V	R, (9) and (10)	R, (9)	8

To extend this modeling framework, we remove the condition (10), thereby increasing the number of independent parameters to four, specifically,  $b_{\sigma}$ ,  $d_{\sigma}$ ,  $b_{\omega}$ , and  $d_{\omega}$ . This modification provides additional flexibility in describing the high-density behavior of symmetric nuclear matter.

For the isovector  $\rho$ -meson, the exponential form (8) with a single parameter  $a_{\rho}$  has been commonly used [66, 69, 72]. In this case, the coupling decreases rapidly with density, approaching zero at high densities.

In the present work, we explore an alternative parametrization of the  $\rho$ -meson coupling by using the rational function (7) with the following three conditions imposed:

$$f(1) = 1, \quad f'(0) = 0, \quad f'(1)/f(1) = f''(1)/f'(1). \quad (11)$$

This leads to a function with one independent parameter (i.e.,  $c_{\rho}$ ), constructed to mimic the low-density behavior of the exponential form. Furthermore, if we also apply the conditions given in (9), the resulting parametrization contains two independent parameters,  $b_{\rho}$  and  $d_{\rho}$ , providing additional flexibility for describing the symmetry energy at high densities.

As alternative parametrizations, one can also construct couplings that depend on the total scalar (S) density  $n_s$ , or a mixed (M) density dependence on  $n_v$  and  $n_s$  simultaneously, where the vector meson couplings  $g_{\omega}$  and  $g_{\rho}$  depend on  $n_v$ , and the scalar meson coupling  $g_{\sigma}$  depends on  $n_s$ , as implemented in Refs. [71, 72].

In the present work, we explore several combinations for the choice of the density entering the argument  $r$ , the functional form of  $f(r)$ , and the conditions imposed on it. Table 1 summarizes these options, using a three-letter abbreviation for identification. The abbreviation indicates, respectively, the type of density used, the functional forms for the two isoscalar mesons ( $\sigma$  and  $\omega$ ), and the functional form for the isovector meson ( $\rho$ ). For example, the DD-ME version recently explored in Refs. [34, 61–64] is abbreviated as “VRE”, indicating a vector density for normalization, a rational function in the isoscalar channel, and an exponential function in the isovector channel. The conditions imposed on the  $f(r)$  functions are made explicit in Table 1.

A further key step is to relate the CDF parameters introduced above to the nuclear characteristic quantities at saturation density. For small isospin asymmetry  $\delta = (n_n - n_p)/n$ , the energy density is decomposed as

$$\varepsilon(n, \delta) \simeq n E_{\text{SNM}}(n) + n E_{\text{sym}}(n) \delta^2, \quad (12)$$

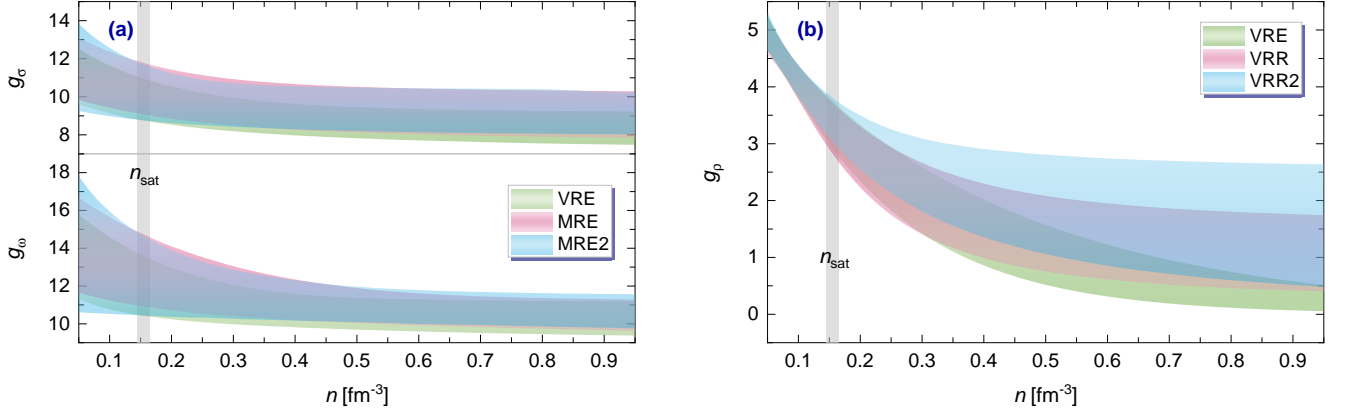


Figure 1: The posterior confidence regions (95.4% CI) for meson-nucleon couplings  $g_\sigma$ ,  $g_\omega$  and  $g_\rho$  obtained using CDFs with different parametrizations for the density dependence. The vertical bands correspond to the saturation density.

where  $E_{\text{SNM}}$  and  $E_{\text{sym}}$  denote the symmetric-matter and symmetry-energy contributions, respectively. These functions are then expanded around saturation density using the dimensionless parameter  $\chi \equiv (n - n_{\text{sat}})/3n_{\text{sat}}$ , in the generic form

$$E_{\text{SNM}}(n) = \sum_{i=0}^4 u_i \chi^i, \quad E_{\text{sym}}(n) = \sum_{i=0}^4 w_i \chi^i. \quad (13)$$

The coefficients  $u_i$  encode the standard empirical characteristics of symmetric nuclear matter:

$$E_{\text{sat}} = u_0, \quad K_{\text{sat}} = 2u_2, \quad Q_{\text{sat}} = 6u_3, \quad Z_{\text{sat}} = 24u_4,$$

corresponding to the saturation energy, incompressibility, skewness, and kurtosis, respectively. Similarly, the coefficients  $w_i$  determine the symmetry-energy characteristics:

$$J_{\text{sym}} = w_0, \quad L_{\text{sym}} = w_1, \quad K_{\text{sym}} = 2w_2, \quad Q_{\text{sym}} = 6w_3, \quad Z_{\text{sym}} = 24w_4,$$

representing the symmetry energy at saturation, its slope, curvature, skewness, and kurtosis.

### 3. Inference framework and constraints

To ensure this presentation is self-contained, we briefly review the Bayesian inference setup of Refs. [34, 61]. The framework incorporates both multi-physics constraints from astrophysical observations and terrestrial experiments, as well as microscopic theory computations, to inform a CDF model of dense matter.

Specifically, for the constraints sensitive to the low-density regime of nucleonic EOS, we consider: (i) a collection of nuclear matter characteristics at saturation  $\{m_D^*, n_{\text{sat}}, E_{\text{sat}}, K_{\text{sat}}, J_{\text{sym}}\}$ , which are well constrained by the low-energy nuclear phenomena [61]; (ii) the energy per particle and pressure for pure neutron matter derived from  $\chi$ EFT interactions [21] within their validity range, i.e., densities below 1.5-2 saturation density. For the astrophysical constraints, we incorporate: (i) the mass measurement of massive pulsars PSR J0348+0432 [79]; (ii) the

tidal deformabilities obtained for the binary neutron star mergers GW170817 and GW190425, by the LIGO-Virgo Collaboration [3, 6]; (iii) the NICER's simultaneous mass and radius estimates for four millisecond pulsars – the  $\sim 2.0 M_\odot$  pulsar PSR J0740+6620 [14], the two canonical mass  $\sim 1.4 M_\odot$  objects PSR J0030+0451 [12] and J0437-4715 [13], and the light  $\sim 1.0 M_\odot$  pulsar PSR J1231-1411 [15]. The constructions of likelihood functions for each constraint are detailed in Refs. [34, 61].

The Bayesian parameters of the CDF model in our analysis include the three coupling strengths ( $g_m$ , with  $m = \sigma, \omega, \rho$ ) at saturation density  $n_{\text{sat}}$ , along with four or five parameters in the functions  $f_m$  that govern their density dependence. Uniform prior distributions are assigned to these parameters over carefully chosen intervals: wide enough to avoid biasing the posterior distributions, yet not so broad as to impede the convergence of the Monte Carlo algorithm.

### 4. Results and implications

To assess the individual impact of each channel of the CDF model on the Bayesian inference, we held the density-dependence of the function  $f(r)$  fixed in one channel (isoscalar or isovector) and varying it in the other, applying identical multi-messenger constraints in all cases.

In Fig. 1, we show the Bayesian inference of the density dependence of the meson-nucleon couplings at 95.4% confidence interval (CI) for each of the CDF models listed in Table 1. In panel (a) the models VRE, MRE, and MRE2 feature different rational functions for the  $\sigma$ - and  $\omega$ -meson couplings, but share the same exponential function  $\rho$ -meson coupling, as does also the VRE model shown in panel (b). By contrast, in panel (b), the models VRE, VRR, and VRR2 feature either rational or exponential functions for the  $\rho$ -meson coupling, but share same rational function for the  $\sigma$ - and  $\omega$ -meson couplings, as does also the VRE model shown in panel (a). The new and updated mass-radius estimates for four pulsars obtained by the NICER collaboration [12–15] are also shown for the sake of reference.

From panel (a) of Fig. 1, one sees that the couplings  $g_\sigma$  and  $g_\omega$  exhibit a self-similar density dependence. This reflects



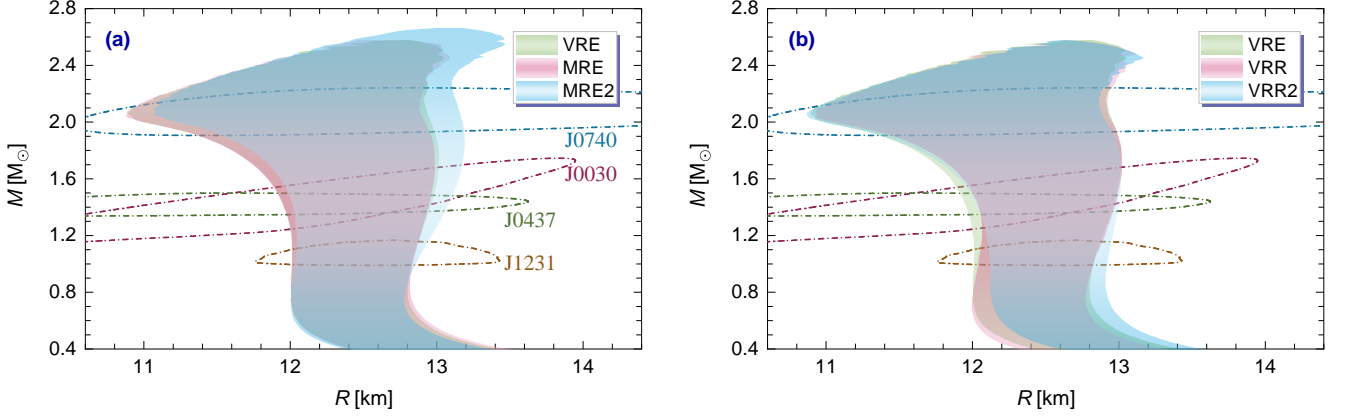


Figure 2: Mass–radius diagram for CSs, with elliptical contours indicating the 95.4% CI regions of mass–radius estimates for four pulsars from NICER observations. Panel (a) shows the posterior 95.4% CI regions obtained using CDFs with different isoscalar coupling parametrizations, while panel (b) presents the results for variations in the isovector coupling.

their complementary roles in Eq. (3):  $g_\sigma$  controls the attractive scalar self-energy  $\Sigma_S$ , while  $g_\omega$  governs the repulsive vector self-energy  $\Sigma_V^n$  through the  $\omega$ -meson field. The delicate balance between  $\Sigma_S$  and  $\Sigma_V^n$  determines the EOS of symmetric nuclear matter.

The range of coupling values spanned by each model determines its flexibility in simultaneously describing different constraints. In panel (b) of Fig. 1, the rational function subject to conditions (11) reproduces the modeling of the  $g_\rho$  coupling with an exponential function at densities up to  $2n_{\text{sat}}$ , but deviates significantly at higher densities. Under conditions (10), the rational function allows much larger  $g_\rho$  values at high densities. Nonetheless, the narrow range and consistency of all three models at and below  $n_{\text{sat}}$  are a consequence of the  $\chi$ EFT constraint for pure neutron matter [34, 61].

The bulk properties of CSs – such as maximum mass, radii, tidal deformabilities, and moments of inertia – are fully determined by the distributions of pressure and energy density throughout the star, as prescribed by the dense matter EOS. Our inferences for the mass-radius diagram of CSs and various thermodynamic quantities of dense matter are shown in Fig. 2–5. Specifically, we show posterior 95.4% confidence regions, whereby we distinguish the results obtained using CDFs with different parametrizations of the isoscalar couplings (left panels) and those with variations in the isovector couplings (right panels). A generic observation that follows from the analysis of results in Figs. 3–5, which will be given below, is that the interplay between isoscalar and isovector channels has a much weaker influence on the thermodynamics of dense matter than the effects of different parametrizations within each respective isospin channel. Below, we discuss the impact of specific parametrizations in detail.

#### 4.1. Influences of parametrizations of isoscalar couplings

We begin by examining the impact of different parametrizations of the isoscalar couplings ( $g_\sigma$  and  $g_\omega$ ) on CS and dense-matter properties. To this end, we compare the posterior distributions obtained with the VRE model against those from the newly introduced MRE and VRE2 models. Figure 2 displays

the posteriors for the mass–radius relation, while Fig. 3 shows the corresponding distributions of the  $\beta$ -equilibrium EOS, together with the particle composition characterized by the proton fraction  $F_p$ , which is fully determined by the density dependence of the symmetry energy.

In both the VRE and MRE models, the number of parameters is sufficient to independently adjust the nuclear characteristics at saturation density up to and including the isoscalar skewness coefficient  $Q_{\text{sat}}$ , and up to the isovector symmetry-energy slope coefficient  $L_{\text{sym}}$  [72, 76]. The left panels of Figs. 2 and 3 demonstrate that the 95.4% CI posteriors for the VRE and MRE models are nearly identical. This consistency is further supported by the behavior of the symmetric nuclear matter EOS and the symmetry energy shown in the left panels of Fig. 4.

The characteristic coefficients of nuclear matter, which quantify its properties around saturation density, are summarized in Fig. 5. We omit the 0th-order coefficients, the saturation energy  $E_{\text{sat}}$ , and the symmetry energy at saturation  $J_{\text{sym}}$ , because they are well constrained and consistent across all models considered in this analysis. For both the VRE and MRE models, the posterior distributions of each displayed coefficient behave similarly and exhibit comparable peak locations. It is important to note, however, that the higher-order coefficients, specifically  $Z_{\text{sat}}$ ,  $K_{\text{sym}}$ , and  $Q_{\text{sym}}$ , are not tunable within the available parametrizations. Instead, their values emerge as predictions of the respective models [72, 76].

The MRE2 model, which includes one additional independent parameter compared to the MRE model, predicts larger radii by approximately 0.1–0.3 km for CSs with masses  $M \gtrsim 1.4 M_\odot$ , along with slightly higher maximum masses  $M_{\text{max}}$  by  $\sim 0.1 M_\odot$ , as shown in panel (a) of Fig. 2. This is because the pulsar PSR J0740+6620, which favors a larger radius, reinforces the selection of EOS that are stiffer at high densities. Correspondingly, the left panels of Fig. 3 indicate that it yields a stiffer  $\beta$ -equilibrium EOS in the relevant density regimes, although the isovector channel, represented by the proton fraction  $F_p$ , remains unaffected. This increased stiffness is also present in the EOS of symmetric nuclear matter at densities  $n \gtrsim 3n_{\text{sat}}$ , as seen in the left panels of Fig. 4. In a recent study, Ref. [64] com-

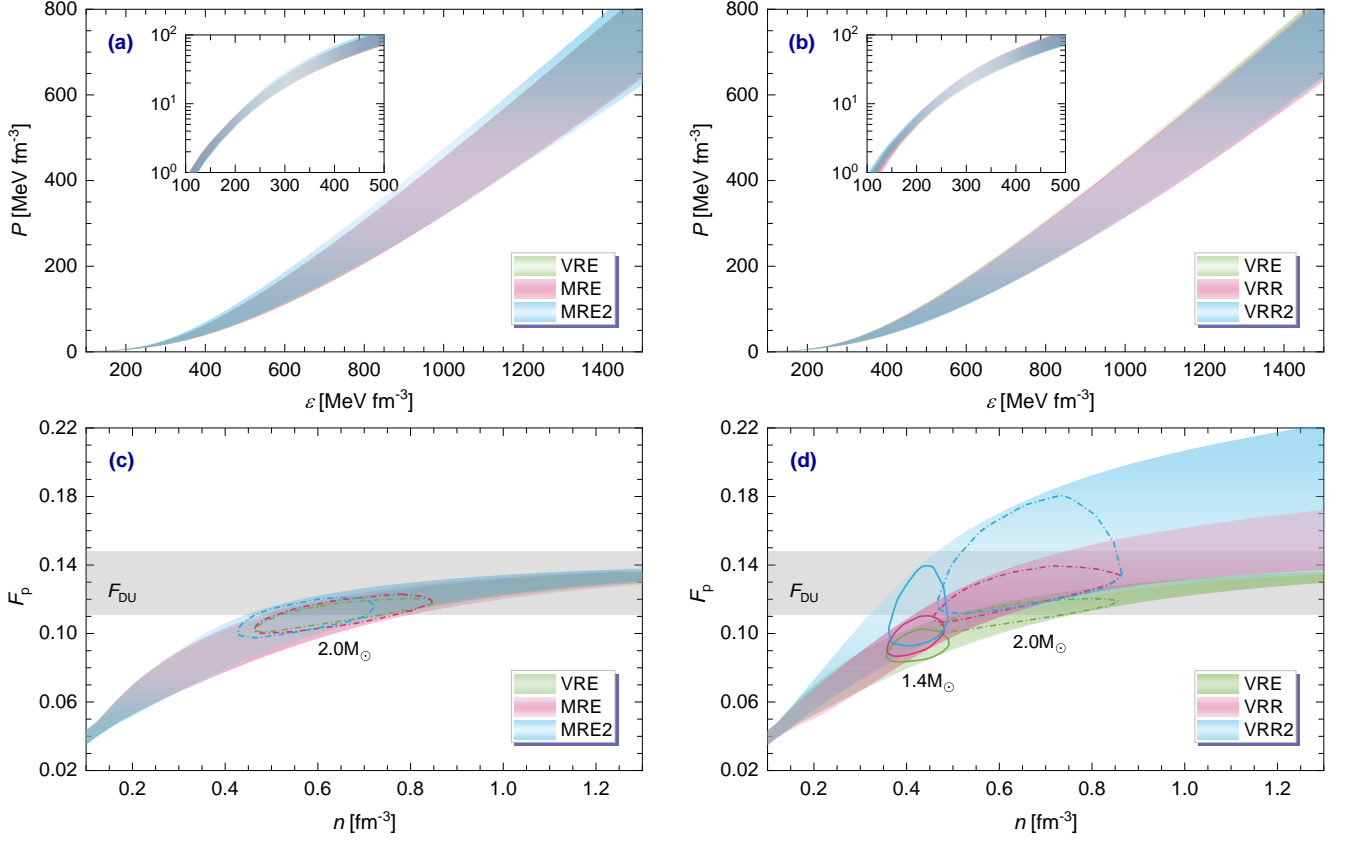


Figure 3: The influences of parametrizations of density-dependent couplings on the  $\beta$ -equilibrium EOS and its particle composition characterized by proton fraction  $F_p$ . Left panels (a and c) show the posterior confidence regions (95.4% CI) obtained using CDFs with different parametrizations of isoscalar couplings, while the right panels (b and d) show the corresponding results for variations in the isovector coupling. In the upper panels, the insets magnify the low-density regime. In the lower panels, the contours show the corresponding distributions of the respective  $1.4$  and  $2.0 M_\odot$  stars, and the horizontal bands labeled  $F_{\text{DU}}$  indicate the admissible proton fraction thresholds for the onset of nuclear direct Urca (DU) cooling process.

pared the computations performed with the VRE model with those that employed simplified functions given by Eq. (8) for the isoscalar couplings, that contain fewer adjustable parameters and therefore have reduced flexibility. This comparison showed that the model with simple exponential dependence predicts larger radii for CSs than the VRE model – a trend that is opposite to our findings. This discrepancy may be attributed to the fact that for the simple exponential representation of the density dependence, the coefficient  $Q_{\text{sat}}$  is not independent, but is constrained by the fits of lower order nuclear characteristics to a large range of values [29].

Because small variations in the incompressibility  $K_{\text{sat}}$  (order-2) have a negligible impact on the high-density EOS [35, 61], the stiffness of the EOS in the MRE2 model arises primarily from the substantially broader distributions of the skewness coefficient  $Q_{\text{sat}}$  (order-3) and the kurtosis coefficient  $Z_{\text{sat}}$  (order-4). As shown in panel (a) of Fig. 5, these distributions are shifted toward larger values compared to the much narrower distributions obtained with the MRE model. Interestingly, all three models predict consistent values for the lower bound (95.4% CI) of  $Q_{\text{sat}}$ .

As is well known, the higher the order of a characteristic coefficient, the farther from  $n_{\text{sat}}$  its influence becomes visible in the behavior of the EOS and related thermodynamic quantities.

At the same time, the assessment of the impact of each specific coefficient is affected by the increasing uncertainty that accompanies higher-order terms. This behavior naturally follows from the Taylor expansion (13): contributions from higher-order coefficients carry progressively smaller weights and, therefore, large variations are needed to cover a prescribed range of priors.

For the MRE2 model, we further examined the correlations between  $Q_{\text{sat}}$  and key CS observables, such as the maximum mass and the radius of a  $2.0 M_\odot$  star. These correlations are relatively strong, with Pearson coefficients of  $r_p \approx 0.7$ - $0.8$ . In contrast, the correlations involving  $Z_{\text{sat}}$  are weak, with  $r_p \approx 0.3$ . Therefore, the skewness coefficient  $Q_{\text{sat}}$  emerges as the most important characteristics of the isoscalar part of the EOS above  $\sim 3 n_{\text{sat}}$  within the density regime relevant for CSs.

#### 4.2. Influences of parametrizations of isovector coupling

We now evaluate the influence of different parametrizations of the isovector coupling ( $g_\rho$ ) on the properties of CSs and dense nuclear matter. We compare the posteriors obtained from the VRE model with those from the newly introduced VRR and VRR2 models.

As shown in panel (b) of Fig. 2, the choice of  $g_\rho$  parametrization has only a modest effect on the global properties of CSs.

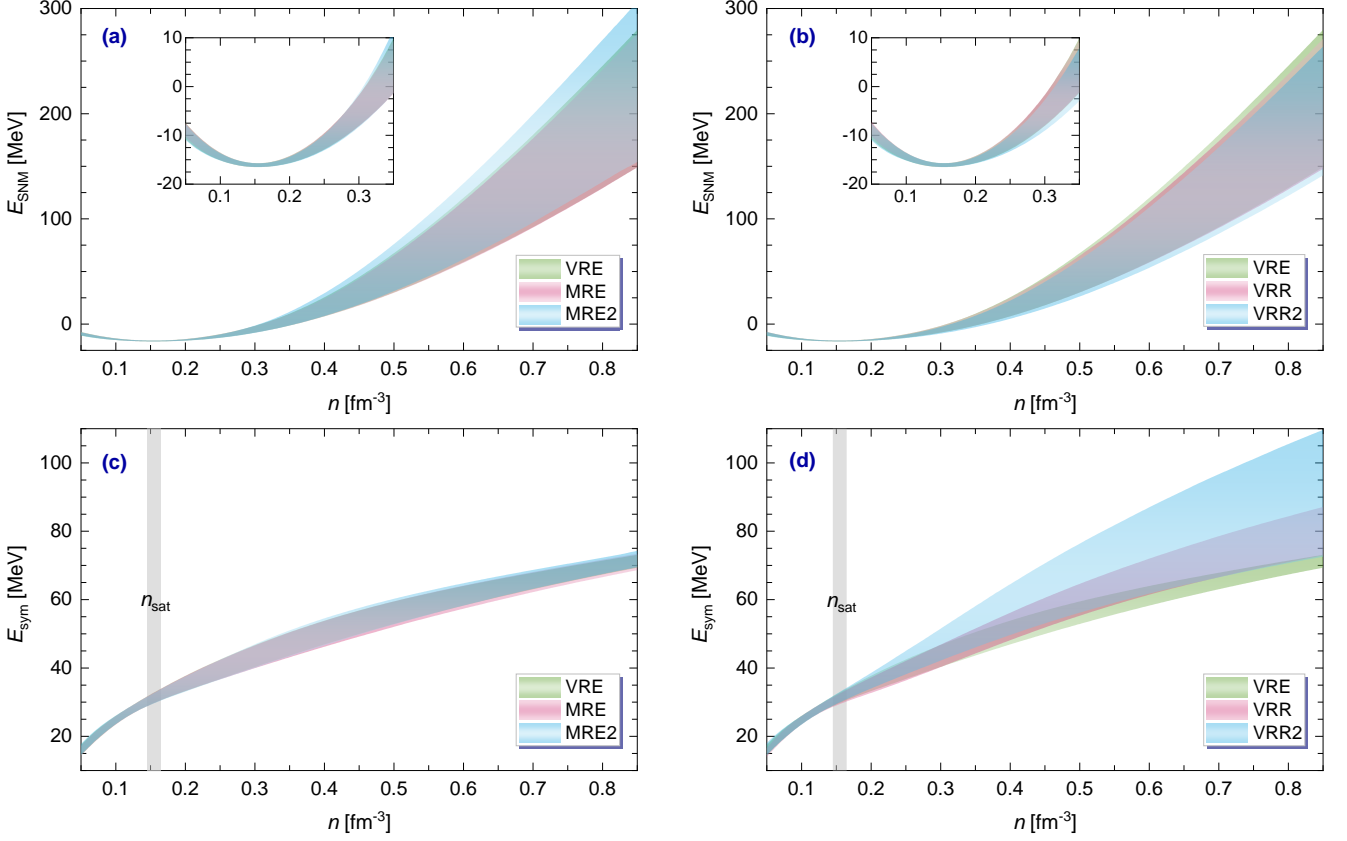


Figure 4: The influences of parametrizations of density-dependent couplings on the energy per particle  $E_{\text{SNM}}$  of symmetric nuclear matter and symmetry energy  $E_{\text{sym}}$ . Left panels (a and c) show the posterior confidence regions (95.4% CI) obtained using CDFs with different parametrizations of isoscalar couplings, while the right panels (b and d) show the results for variations in the isovector coupling. In the upper panels, the insets magnify the low-density regime.

The most noticeable impact occurs for low- to intermediate-mass stars, where the predicted radii vary by approximately 0.1 km in either direction, depending on the model. This behavior arises from modifications to the  $\beta$ -equilibrium EOS at low densities ( $n \lesssim 2n_{\text{sat}}$ ), as illustrated in panel (b) of Fig. 3. These differences are closely tied to small variations in the symmetry-energy slope coefficient  $L_{\text{sym}}$  among the models. In the high-density regime, the posteriors from all three models overlap substantially, despite significant differences in the predicted proton fractions. This indicates that the rational-function parametrizations of  $g_\rho$  introduced in the VRR and VRR2 models primarily modify the high-density behavior of the particle composition, permitting larger proton fractions in the stellar core—a notable departure from the original exponential form used in VRE. These features are qualitatively consistent with the findings of Ref. [64], where an extended exponential function,  $f_\rho(r) = y \exp[-a(r-1)] + (1-y)$  with  $y$  as an additional parameter was employed.

The consistency of the results for the  $\beta$ -equilibrium matter EOS across the three models in the high-density regime can be understood through the decomposition of the energy density of the isospin-asymmetric matter Eq. (12). As shown in the right panels of Fig. 4, a stiffer symmetric-matter EOS may be accompanied by a softer symmetry energy. The latter reduces the proton fraction in dense matter, as illustrated in panel (d) of

Fig. 3, leading to a larger isospin asymmetry  $\delta$ . As a result, the interplay between the isoscalar and isovector channels produces broadly comparable posterior distributions for the pressure and energy density.

These findings indicate that the employed astrophysical constraints in the form of integral parameters of CS (mass, radius, etc.) are only weakly sensitive to the isovector channel of the EOS models. In addition, extracting the symmetry energy and its density dependence from the  $\beta$ -equilibrium EOS carries substantial uncertainties, which are further amplified by model-specific treatments of the isovector channel. This is particularly true for the VRE and VRR models, both of which contain two independent isovector parameters. It should also be emphasized that the dominant uncertainties arise in the high-density regime, whereas the low-density behavior is well constrained by  $\chi$ EFT calculations [34].

In the right panel of Fig. 5, all three models exhibit comparable ranges for the slope coefficient  $L_{\text{sym}}$  (order-1), with median values differing by no more than about 5 MeV. The higher-order coefficients – the curvature  $K_{\text{sym}}$  (order-2) and the skewness  $Q_{\text{sym}}$  (order-3) – therefore provide the main distinctions between the models. However, in the VRE and VRR models, both  $K_{\text{sym}}$  and  $Q_{\text{sym}}$  arise as predictions, since the two independent parameters in the  $g_\rho$  coupling are already tightly constrained by the values of  $J_{\text{sym}}$  and  $L_{\text{sym}}$ . In contrast, the VRR2

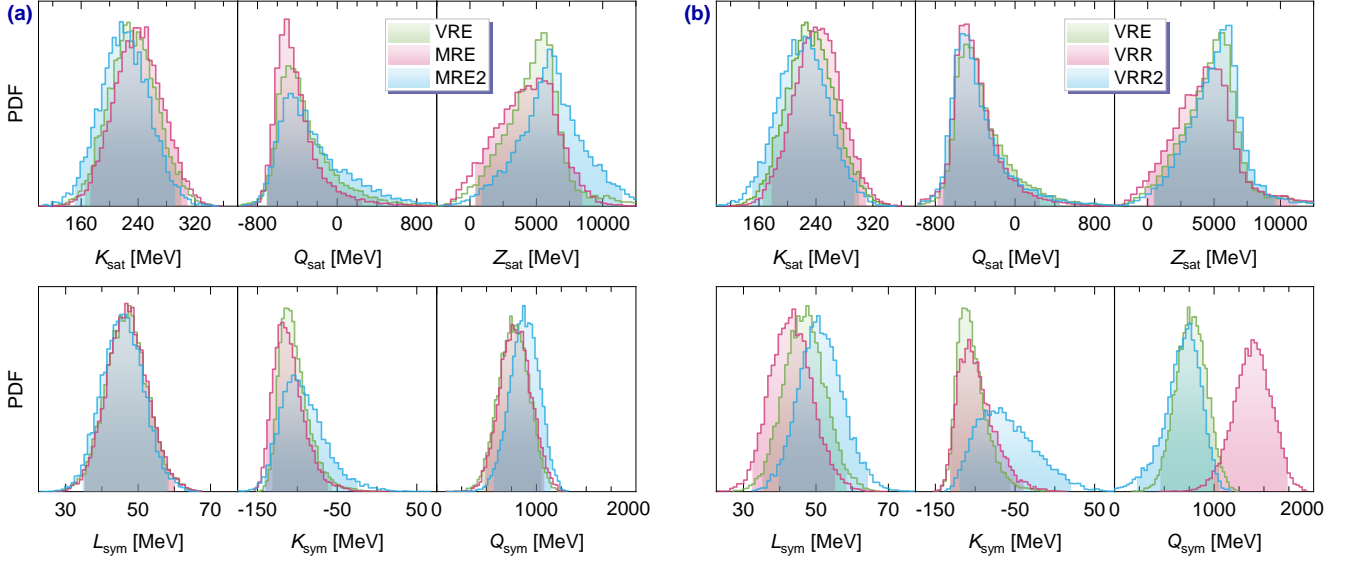


Figure 5: The posterior distributions for the nuclear matter characteristic coefficients at saturation density, where shaded regions correspond to the 95.4% CI. Left panel (a) shows the posteriors obtained using CDFs with different parametrizations of isoscalar couplings; while the right panel (b) shows the results for variations in the isovector coupling.

model introduces a third independent parameter in the  $g_\rho$  coupling, allowing additional freedom to vary  $K_{\text{sym}}$ . Indeed, we find that the correlation between  $L_{\text{sym}}$  and  $K_{\text{sym}}$  is negligible, with a Pearson coefficient of  $r_p \approx 0.1$ .

The VRE and VRR models yield similar posterior distributions for the curvature coefficient  $K_{\text{sym}}$ , but noticeably different distributions for the skewness coefficient  $Q_{\text{sym}}$ . Conversely, the VRE and VRR2 models produce comparable distributions for  $Q_{\text{sym}}$ , while their predictions for  $K_{\text{sym}}$  differ substantially. Taken together with the symmetry energy shown in the lower panels of Fig. 4, these results demonstrate that  $K_{\text{sym}}$  is the most influential nuclear coefficient governing the density dependence of the symmetry energy beyond  $2n_{\text{sat}}$ . The coefficient  $Q_{\text{sym}}$  also contributes significantly, particularly at densities above  $3n_{\text{sat}}$ .

Constraining the nuclear symmetry energy, particularly its high-density behavior, requires complementary strategies to those employed here. Observational data on the surface luminosities of cooling CSs, offer valuable insight into the composition of dense matter and thus into the high-density symmetry energy [80–83]. It is therefore instructive to examine in detail the predicted proton fractions inside CSs across different models, especially regarding the possible onset of the nucleonic direct Urca (DU) process, which, if allowed, would lead to rapid stellar cooling [84–86]. Cooling simulations generally indicate that the DU process should not operate in typical CSs with masses  $M < 1.5 M_\odot$  [80, 87], while various studies have proposed threshold masses in the range of 1.6–1.8  $M_\odot$  for its onset [88–92]. More recently, magneto-thermal simulations of young, cold CSs suggest that viable dense-matter EOSs must permit fast cooling at least within certain mass intervals [93].

In the lower panels of Fig. 3, we also show contours corresponding to CS configurations with 1.4 and 2.0  $M_\odot$ . The horizontal bands indicate the nucleonic DU threshold [94]: the lower limit of 11.1% is obtained from a  $\mu$ -free model, while

the upper limit assumes massless muons—though this applies primarily at high densities. It is evident that the VRE model strongly disfavors the DU process in CSs with  $M \lesssim 2.0 M_\odot$ , consistent with Refs. [34, 64]. In contrast, the VRR2 model permits the DU process even in stars with masses as low as 1.4  $M_\odot$ , while the VRR model yields intermediate predictions. These results suggest that the present rational-function parametrizations of the  $\rho$ -meson coupling warrant further applications in studies of cold CSs and, by extension, also supernova and binary neutron star merger matter.

## 5. Conclusions

In this work, we performed a systematic comparison of Bayesian inference outcomes for CDF-type EOS of dense matter, with a particular focus on the influence of different functional forms describing vector- or scalar-density dependence beyond the standard assumptions. All CDF models were constrained by the same set of nuclear and astrophysical observables, using identical methods to construct the likelihood functions. The prior intervals for the CDF parameters were chosen to be sufficiently wide to avoid biasing the posterior distributions.

Our analysis evaluated the resulting differences in inferences by examining the properties of CSs and dense matter, along with the particle composition. We found that CDF models featuring the same functional form of density dependence – but differing in the type of density (vector or scalar) employed in the density-parametrization – yield nearly identical posterior results for the global properties of CSs (such as maximum mass, radii, and tidal deformabilities) and dense matter (including the EOS, nuclear characteristic coefficients, and particle composition) with the 95.4% CI essentially overlapping.

Extending the functional form of the density dependence in the isoscalar channel to achieve greater flexibility primar-



ily affects dense matter at high densities: while its impact on global CS properties are modest, the proton fraction in massive stars can be significantly unaltered. Consequently, CDFs that allow the nuclear saturation characteristics in the isoscalar channel, including the skewness coefficient  $Q_{\text{sat}}$ , to be freely adjusted provide a robust framework for modeling nuclear and CS matter. Our Bayesian analysis further shows that different functional forms in the isovector channel yield comparable posterior results for the bulk properties of CSs, but lead to notable differences in the density dependence of the symmetry energy and, correspondingly, in the particle composition of dense matter. This underscores that probing the nuclear symmetry energy at high densities requires an alternative strategies, such as studying CS cooling. The rational-function parametrization of the isovector meson coupling introduced here incorporates two independent parameters, enabling flexible tuning of nuclear saturation properties, such as the curvature coefficient  $K_{\text{sym}}$ . This approach provides a suitable framework for future simulations of CSs and heavy-ion collisions aimed at probing the effects due to isospin asymmetry.

### Acknowledgments

G. W. and J. L. acknowledge the support of the National Natural Science Foundation of China under Grant No. 12475150. A. S. is supported by the Deutsche Forschungsgemeinschaft (DFG) under Grant No. SE 1836/6-1 and by the Polish National Science Centre (NCN) under Grant No. 2023/51/B/ST9/02798. Y. W. and Q. L. are supported by the National Natural Science Foundation of China (Grant Nos. 12335008 and 12505143), the National Key Research and Development Program of China (Grant Nos. 2023YFA1606402 and 2022YFE0103400).

### Declaration of competing interest

The authors declare that they have no known competing financial interests or personal relationships that could have appeared to influence the work reported in this paper.

### Data availability

Data will be made available on request.

### References

- [1] M. Oertel, M. Hempel, T. Klähn, S. Typel, Equations of state for supernovae and compact stars, *Rev. Mod. Phys.* 89 (2017) 015007. [arXiv:1610.03361](#), [doi:10.1103/RevModPhys.89.015007](#).
- [2] A. Sedrakian, J. J. Li, F. Weber, Heavy baryons in compact stars, *Prog. Part. Nucl. Phys.* 131 (2023) 104041. [arXiv:2212.01086](#), [doi:10.1016/j.ppnp.2023.104041](#).
- [3] B. P. Abbott, R. Abbott, T. D. Abbott, et al., GW170817: Observation of Gravitational Waves from a Binary Neutron Star Inspiral, *Phys. Rev. Lett.* 119 (2017) 161101. [arXiv:1710.05832](#), [doi:10.1103/PhysRevLett.119.161101](#).
- [4] B. P. Abbott, R. Abbott, T. D. Abbott, et al., GW170817: Measurements of neutron star radii and equation of state, *Phys. Rev. Lett.* 121 (2018) 161101. [arXiv:1805.11581](#), [doi:10.1103/PhysRevLett.121.161101](#).
- [5] B. P. Abbott, R. Abbott, T. D. Abbott, et al., Properties of the binary neutron star merger GW170817, *Phys. Rev. X* 9 (2019) 011001. [arXiv:1805.11579](#), [doi:10.1103/PhysRevX.9.011001](#).
- [6] B. P. Abbott, R. Abbott, T. D. Abbott, et al., GW190425: Observation of a Compact Binary Coalescence with Total Mass  $\sim 3.4M_{\odot}$ , *Astrophys. J. Lett.* 892 (2020) L3. [arXiv:2001.01761](#), [doi:10.3847/2041-8213/ab75f5](#).
- [7] R. Abbott, T. D. Abbott, S. Abraham, et al., GW190814: Gravitational Waves from the Coalescence of a 23 Solar Mass Black Hole with a 2.6 Solar Mass Compact Object, *Astrophys. J. Lett.* 896 (2020) L44. [arXiv:2006.12611](#), [doi:10.3847/2041-8213/ab960f](#).
- [8] T. E. Riley, A. L. Watts, S. Bogdanov, et al., A *NICER* View of PSR J0030+0451: Millisecond Pulsar Parameter Estimation, *Astrophys. J. Lett.* 887 (2019) L21. [arXiv:1912.05702](#), [doi:10.3847/2041-8213/ab481c](#).
- [9] T. E. Riley, A. L. Watts, P. S. Ray, et al., A *NICER* View of the Massive Pulsar PSR J0740+6620 Informed by Radio Timing and XMM-Newton Spectroscopy, *Astrophys. J. Lett.* 918 (2021) L27. [arXiv:2105.06980](#), [doi:10.3847/2041-8213/ac0a81](#).
- [10] M. C. Miller, F. K. Lamb, A. J. Dittmann, et al., PSR J0030+0451 Mass and Radius from *NICER* Data and Implications for the Properties of Neutron Star Matter, *Astrophys. J. Lett.* 887 (2019) L24. [arXiv:1912.05705](#), [doi:10.3847/2041-8213/ab50c5](#).
- [11] M. C. Miller, F. K. Lamb, A. J. Dittmann, et al., The Radius of PSR J0740+6620 from *NICER* and XMM-Newton Data, *Astrophys. J. Lett.* 918 (2021) L28. [arXiv:2105.06979](#), [doi:10.3847/2041-8213/ac089b](#).
- [12] S. Vinciguerra, T. Salmi, A. L. Watts, et al., An Updated Mass–Radius Analysis of the 2017–2018 *NICER* Data Set of PSR J0030+0451, *Astrophys. J.* 961 (2024) 62. [arXiv:2308.09469](#), [doi:10.3847/1538-4357/acfb83](#).
- [13] D. Choudhury, T. Salmi, S. Vinciguerra, et al., A *NICER* View of the Nearest and Brightest Millisecond Pulsar: PSR J0437–4715, *Astrophys. J. Lett.* 971 (2024) L20. [arXiv:2407.06789](#), [doi:10.3847/2041-8213/ad5a6f](#).

- [14] T. Salmi, D. Choudhury, Y. Kini, et al., The Radius of the High-mass Pulsar PSR J0740+6620 with 3.6 yr of NICER Data, *Astrophys. J.* 974 (2024) 294. [arXiv:2406.14466](#), [doi:10.3847/1538-4357/ad5f1f](#).
- [15] T. Salmi, J. S. Deneva, P. S. Ray, et al., A NICER View of PSR J1231-1411: A Complex Case, *Astrophys. J.* 976 (2024) 58. [arXiv:2409.14923](#), [doi:10.3847/1538-4357/ad81d2](#).
- [16] L. Mauviard, S. Guillot, T. Salmi, et al., A NICER view of the 1.4 solar-mass edge-on pulsar PSR J0614–3329, *arXiv* (2025) 2506.14883 [arXiv:2506.14883](#).
- [17] D. Adhikari, H. Albataineh, D. Androic, et al., Accurate Determination of the Neutron Skin Thickness of  $^{208}\text{Pb}$  through Parity-Violation in Electron Scattering, *Phys. Rev. Lett.* 126 (2021) 172502. [arXiv:2102.10767](#), [doi:10.1103/PhysRevLett.126.172502](#).
- [18] D. Adhikari, H. Albataineh, D. Androic, et al., Precision Determination of the Neutral Weak Form Factor of  $\text{Ca}^{48}$ , *Phys. Rev. Lett.* 129 (2022) 042501. [arXiv:2205.11593](#), [doi:10.1103/PhysRevLett.129.042501](#).
- [19] B. T. Reed, F. J. Fattoyev, C. J. Horowitz, J. Piekarewicz, Implications of PREX-2 on the Equation of State of Neutron-Rich Matter, *Phys. Rev. Lett.* 126 (2021) 172503. [arXiv:2101.03193](#), [doi:10.1103/PhysRevLett.126.172503](#).
- [20] P.-G. Reinhard, X. Roca-Maza, W. Nazarewicz, Information Content of the Parity-Violating Asymmetry in  $\text{Pb}^{208}$ , *Phys. Rev. Lett.* 127 (2021) 232501. [arXiv:2105.15050](#), [doi:10.1103/PhysRevLett.127.232501](#).
- [21] K. Hebeler, J. M. Lattimer, C. J. Pethick, A. Schwenk, Equation of state and neutron star properties constrained by nuclear physics and observation, *Astrophys. J.* 773 (2013) 11. [arXiv:1303.4662](#), [doi:10.1088/0004-637X/773/1/11](#).
- [22] J. E. Lynn, I. Tews, J. Carlson, S. Gandolfi, A. Gezerlis, K. E. Schmidt, A. Schwenk, Chiral Three-Nucleon Interactions in Light Nuclei, Neutron- $\alpha$  Scattering, and Neutron Matter, *Phys. Rev. Lett.* 116 (2016) 062501. [arXiv:1509.03470](#), [doi:10.1103/PhysRevLett.116.062501](#).
- [23] C. Drischler, K. Hebeler, A. Schwenk, Chiral interactions up to next-to-next-to-next-to-leading order and nuclear saturation, *Phys. Rev. Lett.* 122 (2019) 042501. [arXiv:1710.08220](#), [doi:10.1103/PhysRevLett.122.042501](#).
- [24] J. Keller, K. Hebeler, A. Schwenk, Nuclear Equation of State for Arbitrary Proton Fraction and Temperature Based on Chiral Effective Field Theory and a Gaussian Process Emulator, *Phys. Rev. Lett.* 130 (2023) 072701. [arXiv:2204.14016](#), [doi:10.1103/PhysRevLett.130.072701](#).
- [25] O. Komoltsev, A. Kurkela, How Perturbative QCD Constrains the Equation of State at Neutron-Star Densities, *Phys. Rev. Lett.* 128 (2022) 202701. [arXiv:2111.05350](#), [doi:10.1103/PhysRevLett.128.202701](#).
- [26] L. Brandes, W. Weise, N. Kaiser, Evidence against a strong first-order phase transition in neutron star cores: Impact of new data, *Phys. Rev. D* 108 (2023) 094014. [arXiv:2306.06218](#), [doi:10.1103/PhysRevD.108.094014](#).
- [27] T. Gorda, O. Komoltsev, A. Kurkela, Ab-initio QCD Calculations Impact the Inference of the Neutron-star-matter Equation of State, *Astrophys. J.* 950 (2023) 107. [arXiv:2204.11877](#), [doi:10.3847/1538-4357/acce3a](#).
- [28] S. Traversi, P. Char, G. Pagliara, Bayesian Inference of Dense Matter Equation of State within Relativistic Mean Field Models using Astrophysical Measurements, *Astrophys. J.* 897 (2020) 165. [arXiv:2002.08951](#), [doi:10.3847/1538-4357/ab99c1](#).
- [29] T. Malik, M. Ferreira, B. K. Agrawal, C. Providência, Relativistic Description of Dense Matter Equation of State and Compatibility with Neutron Star Observables: A Bayesian Approach, *Astrophys. J.* 930 (2022) 17. [arXiv:2201.12552](#), [doi:10.3847/1538-4357/ac5d3c](#).
- [30] T. Malik, B. K. Agrawal, C. Providência, Inferring the nuclear symmetry energy at suprasaturation density from neutrino cooling, *Phys. Rev. C* 106 (2022) L042801. [arXiv:2206.15404](#), [doi:10.1103/PhysRevC.106.L042801](#).
- [31] M. V. Beznogov, A. R. Raduta, Bayesian Survey of the Dense Matter Equation of State Built upon Skyrme Effective Interactions, *Astrophys. J.* 966 (2024) 216. [arXiv:2308.15351](#), [doi:10.3847/1538-4357/ad2f9b](#).
- [32] M. V. Beznogov, A. R. Raduta, Bayesian inference of the dense matter equation of state built upon extended Skyrme interactions, *Phys. Rev. C* 110 (2024) 035805. [arXiv:2403.19325](#), [doi:10.1103/PhysRevC.110.035805](#).
- [33] C. Huang, G. Raaijmakers, A. L. Watts, L. Tolos, C. Providência, Constraining a relativistic mean field model using neutron star mass–radius measurements I: nucleonic models, *Mon. Not. R. Astron. Soc.* 529 (2024) 4650–4665. [arXiv:2303.17518](#), [doi:10.1093/mnras/stae844](#).
- [34] J.-J. Li, Y. Tian, A. Sedrakian, Bayesian constraints on covariant density functional equations of state of compact stars with new NICER mass-radius measurements, *Phys. Lett. B* 865 (2025) 139501. [arXiv:2412.16513](#), [doi:10.1016/j.physletb.2025.139501](#).
- [35] J. Margueron, R. Hoffmann Casali, F. Gulminelli, Equation of state for dense nucleonic matter from metamodeling. II. Predictions for neutron star properties, *Phys.*

- Rev. C 97 (2018) 025806. [arXiv:1708.06895](#), [doi:10.1103/PhysRevC.97.025806](#).
- [36] N.-B. Zhang, B.-A. Li, GW190814's Secondary Component with Mass  $2.50\text{--}2.67 M_{\odot}$  as a Superfast Pulsar, *Astrophys. J.* 902 (2020) 38. [arXiv:2007.02513](#), [doi:10.3847/1538-4357/abb470](#).
- [37] C. Y. Tsang, M. B. Tsang, W. G. Lynch, R. Kumar, C. J. Horowitz, Determination of the equation of state from nuclear experiments and neutron star observations, *Nature Astron.* 8 (2024) 328–336. [arXiv:2310.11588](#), [doi:10.1038/s41550-023-02161-z](#).
- [38] J. Margueron, C. Drischler, M. Dutra, et al., The nucleardatapy toolkit for simple access to experimental nuclear data, astrophysical observations, and theoretical predictions, *arXiv* (2025) 2506.20434 [arXiv:2506.20434](#).
- [39] G. Raaijmakers, T. E. Riley, A. L. Watts, et al., A *NICER* view of PSR J0030+0451: Implications for the dense matter equation of state, *Astrophys. J. Lett.* 887 (2019) L22. [arXiv:1912.05703](#), [doi:10.3847/2041-8213/ab451a](#).
- [40] P. Landry, R. Essick, K. Chatziioannou, Nonparametric constraints on neutron star matter with existing and upcoming gravitational wave and pulsar observations, *Phys. Rev. D* 101 (2020) 123007. [arXiv:2003.04880](#), [doi:10.1103/PhysRevD.101.123007](#).
- [41] I. Legred, K. Chatziioannou, R. Essick, S. Han, P. Landry, Impact of the PSR J0740+6620 radius constraint on the properties of high-density matter, *Phys. Rev. D* 104 (2021) 063003. [arXiv:2106.05313](#), [doi:10.1103/PhysRevD.104.063003](#).
- [42] P. T. H. Pang, I. Tews, M. W. Coughlin, et al., Nuclear Physics Multimessenger Astrophysics Constraints on the Neutron Star Equation of State: Adding *NICER*'s PSR J0740+6620 Measurement, *Astrophys. J.* 922 (2021) 14. [arXiv:2105.08688](#), [doi:10.3847/1538-4357/ac19ab](#).
- [43] S. Altiparmak, C. Ecker, L. Rezzolla, On the Sound Speed in Neutron Stars, *Astrophys. J. Lett.* 939 (2022) L34. [arXiv:2203.14974](#), [doi:10.3847/2041-8213/ac9b2a](#).
- [44] E. Annala, T. Gorda, E. Katerini, A. Kurkela, J. Nättilä, V. Paschalidis, A. Vuorinen, Multimessenger Constraints for Ultradense Matter, *Phys. Rev. X* 12 (2022) 011058. [arXiv:2105.05132](#), [doi:10.1103/PhysRevX.12.011058](#).
- [45] E. V. Chimanski, R. V. Lobato, A. R. Goncalves, C. A. Bertulani, Bayesian Exploration of Phenomenological EoS of Neutron/Hybrid Stars with Recent Observations, *Parti.* 6 (2023) 198–216. [arXiv:2205.01174](#), [doi:10.3390/particles6010011](#).
- [46] N. Rutherford, M. Mendes, I. Svensson, et al., Constraining the Dense Matter Equation of State with New *NICER* Mass–Radius Measurements and New Chiral Effective Field Theory Inputs, *Astrophys. J. Lett.* 971 (2024) L19. [arXiv:2407.06790](#), [doi:10.3847/2041-8213/ad5f02](#).
- [47] Y.-Z. Fan, M.-Z. Han, J.-L. Jiang, D.-S. Shao, S.-P. Tang, Maximum gravitational mass  $M_{\text{TOV}} = 2.25^{+0.08}_{-0.07} M_{\odot}$  inferred at about 3% precision with multimessenger data of neutron stars, *Phys. Rev. D* 109 (2024) 043052. [arXiv:2309.12644](#), [doi:10.1103/PhysRevD.109.043052](#).
- [48] D. Vretenar, A. V. Afanasjev, G. A. Lalazissis, P. Ring, Relativistic Hartree Bogoliubov theory: static and dynamic aspects of exotic nuclear structure, *Phys. Rept.* 409 (2005) 101–259. [doi:10.1016/j.physrep.2004.10.001](#).
- [49] T. Niksic, D. Vretenar, P. Ring, Relativistic Nuclear Energy Density Functionals: Mean-Field and Beyond, *Prog. Part. Nucl. Phys.* 66 (2011) 519–548. [arXiv:1102.4193](#), [doi:10.1016/j.ppnp.2011.01.055](#).
- [50] J. Yang, J. Piekarewicz, Covariant Density Functional Theory in Nuclear Physics and Astrophysics, *Ann. Rev. Nucl. Part. Sci.* 70 (2020) 21–41. [arXiv:1912.11112](#), [doi:10.1146/annurev-nucl-101918-023608](#).
- [51] Z. Zhu, A. Li, T. Liu, A Bayesian Inference of a Relativistic Mean-field Model of Neutron Star Matter from Observations of *NICER* and GW170817/AT2017gfo, *Astrophys. J.* 943 (2023) 163. [arXiv:2211.02007](#), [doi:10.3847/1538-4357/acac1f](#).
- [52] C. Providência, T. Malik, M. B. Albino, M. Ferreira, Neutron star equation of state: identifying hadronic matter characteristics, *arXiv* (2023) 2307.05086 [arXiv:2307.05086](#), [doi:10.1201/9781003306580-5](#).
- [53] P. Char, C. Mondal, F. Gulminelli, M. Oertel, Generalized description of neutron star matter with a nucleonic relativistic density functional, *Phys. Rev. D* 108 (2023) 103045. [arXiv:2307.12364](#), [doi:10.1103/PhysRevD.108.103045](#).
- [54] M. V. Beznogov, A. R. Raduta, Bayesian inference of the dense matter equation of state built upon covariant density functionals, *Phys. Rev. C* 107 (2023) 045803. [arXiv:2212.07168](#), [doi:10.1103/PhysRevC.107.045803](#).
- [55] T. Malik, M. Ferreira, M. B. Albino, C. Providência, Spanning the full range of neutron star properties within a microscopic description, *Phys. Rev. D* 107 (2023) 103018. [arXiv:2301.08169](#), [doi:10.1103/PhysRevD.107.103018](#).
- [56] M. Salinas, J. Piekarewicz, Bayesian refinement of covariant energy density functionals, *Phys. Rev. C* 107 (2023) 045802. [arXiv:2301.09692](#), [doi:10.1103/PhysRevC.107.045802](#).

- [57] C. Mondal, F. Gulminelli, Nucleonic metamodeling in light of multimessenger, PREX-II, and CREX data, *Phys. Rev. C* 107 (2023) 015801. [arXiv:2209.05177](#), [doi:10.1103/PhysRevC.107.015801](#).
- [58] J. Zhou, J. Xu, P. Papakonstantinou, Bayesian inference of neutron-star observables based on effective nuclear interactions, *Phys. Rev. C* 107 (2023) 055803. [arXiv:2301.07904](#), [doi:10.1103/PhysRevC.107.055803](#).
- [59] V. Parmar, V. B. Thapa, A. Kumar, D. Bandyopadhyay, M. Sinha, Bayesian inference of the dense-matter equation of state of neutron stars with antikaon condensation, *Phys. Rev. C* 110 (2024) 045804. [arXiv:2409.19451](#), [doi:10.1103/PhysRevC.110.045804](#).
- [60] L. Scurto, H. Pais, F. Gulminelli, General predictions of neutron star properties using unified relativistic mean-field equations of state, *Phys. Rev. D* 109 (2024) 103015. [arXiv:2402.15548](#), [doi:10.1103/PhysRevD.109.103015](#).
- [61] J.-J. Li, Y. Tian, A. Sedrakian, Bayesian inferences on covariant density functionals from multimessenger astrophysical data: Nucleonic models, *Phys. Rev. C* 111 (2025) 055804. [arXiv:2502.20000](#), [doi:10.1103/PhysRevC.111.055804](#).
- [62] J.-J. Li, A. Sedrakian, Bayesian inferences on covariant density functionals from multimessenger astrophysical data: The impacts of likelihood functions of low density matter constraints, *Phys. Rev. C* 112 (2025) 015802. [arXiv:2505.00911](#), [doi:10.1103/c1k3-k415](#).
- [63] P. Char, C. Mondal, Exploring the limits of nucleonic metamodeling using different relativistic density functionals, *Phys. Rev. D* 111 (2025) 103024. [arXiv:2502.04211](#), [doi:10.1103/PhysRevD.111.103024](#).
- [64] J. Cartaxo, C. Huang, T. Malik, et al., Covariant Energy Density Functionals for Neutron Star Matter Equation of State Modeling: Cross-Comparison Analysis Using CompactObject, *arXiv* (2025) 2506.03112 [arXiv:2506.03112](#).
- [65] C. Fuchs, H. Lenske, H. H. Wolter, Density dependent hadron field theory, *Phys. Rev. C* 52 (1995) 3043–3060. [arXiv:nucl-th/9507044](#), [doi:10.1103/PhysRevC.52.3043](#).
- [66] S. Typel, H. H. Wolter, Relativistic mean field calculations with density dependent meson nucleon coupling, *Nucl. Phys. A* 656 (1999) 331–364. [doi:10.1016/S0375-9474\(99\)00310-3](#).
- [67] F. Hofmann, C. M. Keil, H. Lenske, Density dependent hadron field theory for asymmetric nuclear matter and exotic nuclei, *Phys. Rev. C* 64 (2001) 034314. [arXiv:nucl-th/0007050](#), [doi:10.1103/PhysRevC.64.034314](#).
- [68] Q. Li, Z. Li, E. Zhao, Density and temperature dependence of nucleon nucleon elastic cross-section, *Phys. Rev. C* 69 (2004) 017601. [arXiv:nucl-th/0312098](#), [doi:10.1103/PhysRevC.69.017601](#).
- [69] G. A. Lalazissis, T. Niksic, D. Vretenar, P. Ring, New relativistic mean-field interaction with density-dependent meson-nucleon couplings, *Phys. Rev. C* 71 (2005) 024312. [doi:10.1103/PhysRevC.71.024312](#).
- [70] P. Gogelein, E. N. E. van Dalen, C. Fuchs, H. Muther, Nuclear matter in the crust of neutron stars derived from realistic NN interactions, *Phys. Rev. C* 77 (2008) 025802. [arXiv:0708.2867](#), [doi:10.1103/PhysRevC.77.025802](#).
- [71] S. Typel, Relativistic Mean-Field Models with Different Parametrizations of Density Dependent Couplings, *Parti.* 1 (2018) 3–22. [doi:10.3390/particles1010002](#).
- [72] J. J. Li, A. Sedrakian, New Covariant Density Functionals of Nuclear Matter for Compact Star Simulations, *Astrophys. J.* 957 (2023) 41. [arXiv:2308.14457](#), [doi:10.3847/1538-4357/acfa73](#).
- [73] M. Nan, P. Li, W. Zuo, Q. Li, Nucleon- $\Delta$  elastic cross section in isospin-asymmetric nuclear medium with inclusion of scalar-isovector  $\delta$  meson field, *Chin. Phys. C* 49 (2025) 094112. [arXiv:2412.13497](#), [doi:10.1088/1674-1137/add8fd](#).
- [74] A. Shrivastava, P. Char, S. Gautam, S. Banik, Systematic study of scalar, vector, and mixed density dependencies in relativistic mean-field descriptions of hyperonic matter in neutron stars, *arXiv* (2025) 2511.01505 [arXiv:2511.01505](#).
- [75] J. J. Li, A. Sedrakian, Constraining compact star properties with nuclear saturation parameters, *Phys. Rev. C* 100 (2019) 015809. [arXiv:1903.06057](#), [doi:10.1103/PhysRevC.100.015809](#).
- [76] J. J. Li, A. Sedrakian, Implications from GW170817 for  $\Delta$ -isobar Admixed Hypernuclear Compact Stars, *Astrophys. J. Lett.* 874 (2019) L22. [arXiv:1904.02006](#), [doi:10.3847/2041-8213/ab1090](#).
- [77] J. J. Li, W. H. Long, A. Sedrakian, Hypernuclear stars from relativistic Hartree-Fock density functional theory, *Eur. Phys. J. A* 54 (2018) 133. [arXiv:1801.07084](#), [doi:10.1140/epja/i2018-12566-6](#).
- [78] E. N. E. van Dalen, C. Fuchs, A. Faessler, Dirac-Brueckner-Hartree-Fock calculations for isospin asymmetric nuclear matter based on improved approximation schemes, *Eur. Phys. J. A* 31 (2007) 29–42. [arXiv:nucl-th/0612066](#), [doi:10.1140/epja/i2006-10165-x](#).



- [79] J. Antoniadis, P. C. C. Freire, N. Wex, et al., A Massive Pulsar in a Compact Relativistic Binary, *Science* 340 (2013) 6131. [arXiv:1304.6875](#), [doi:10.1126/science.1233232](#).
- [80] D. Blaschke, H. Grigorian, D. N. Voskresensky, Cooling of neutron stars: Hadronic model, *Astron. Astrophys.* 424 (2004) 979–992. [arXiv:astro-ph/0403170](#), [doi:10.1051/0004-6361:20040404](#).
- [81] D. Page, U. Geppert, F. Weber, The Cooling of compact stars, *Nucl. Phys. A* 777 (2006) 497–530. [arXiv:astro-ph/0508056](#), [doi:10.1016/j.nuclphysa.2005.09.019](#).
- [82] D. Page, M. Prakash, J. M. Lattimer, A. W. Steiner, Rapid Cooling of the Neutron Star in Cassiopeia A Triggered by Neutron Superfluidity in Dense Matter, *Phys. Rev. Lett.* 106 (2011) 081101. [arXiv:1011.6142](#), [doi:10.1103/PhysRevLett.106.081101](#).
- [83] A. Y. Potekhin, J. A. Pons, D. Page, Neutron stars - cooling and transport, *Space Sci. Rev.* 191 (2015) 239–291. [arXiv:1507.06186](#), [doi:10.1007/s11214-015-0180-9](#).
- [84] J. M. Lattimer, M. Prakash, C. J. Pethick, P. Haensel, Direct URCA process in neutron stars, *Phys. Rev. Lett.* 66 (1991) 2701–2704. [doi:10.1103/PhysRevLett.66.2701](#).
- [85] M. Prakash, M. Prakash, J. M. Lattimer, C. J. Pethick, Rapid cooling of neutron stars by hyperons and Delta isobars, *Astrophys. J. Lett.* 390 (1992) L77. [doi:10.1086/186376](#).
- [86] C. Schaab, D. Voskresensky, A. D. Sedrakian, F. Weber, M. K. Weigel, Impact of medium effects on the cooling of nonsuperfluid and superfluid neutron stars, *Astron. Astrophys.* 321 (1997) 591. [arXiv:astro-ph/9605188](#).
- [87] S. Popov, H. Grigorian, R. Turolla, D. Blaschke, Population synthesis as a probe of neutron star thermal evolution, *Astron. Astrophys.* 448 (2006) 327. [arXiv:astro-ph/0411618](#), [doi:10.1051/0004-6361:20042412](#).
- [88] E. F. Brown, A. Cumming, Mapping crustal heating with the cooling lightcurves of quasi-persistent transients, *Astrophys. J.* 698 (2009) 1020–1032. [arXiv:0901.3115](#), [doi:10.1088/0004-637X/698/2/1020](#).
- [89] M. V. Beznogov, D. G. Yakovlev, Statistical theory of thermal evolution of neutron stars, *Mon. Not. Roy. Astron. Soc.* 447 (2015) 1598–1609. [arXiv:1411.6803](#), [doi:10.1093/mnras/stu2506](#).
- [90] M. V. Beznogov, D. G. Yakovlev, Statistical theory of thermal evolution of neutron stars – II. Limitations on direct Urca threshold, *Mon. Not. Roy. Astron. Soc.* 452 (2015) 540–548. [arXiv:1507.04206](#), [doi:10.1093/mnras/stv1293](#).
- [91] E. F. Brown, A. Cumming, F. J. Fattoyev, C. J. Horowitz, D. Page, S. Reddy, Rapid neutrino cooling in the neutron star MXB 1659-29, *Phys. Rev. Lett.* 120 (2018) 182701. [arXiv:1801.00041](#), [doi:10.1103/PhysRevLett.120.182701](#).
- [92] S. Beloin, S. Han, A. W. Steiner, K. Odbadrakh, Simultaneous Fitting of Neutron Star Structure and Cooling Data, *Phys. Rev. C* 100 (2019) 055801. [arXiv:1812.00494](#), [doi:10.1103/PhysRevC.100.055801](#).
- [93] A. Marino, C. Dehman, K. Kovlakas, N. Rea, J. A. Pons, D. Viganò, Constraints on the dense matter equation of state from young and cold isolated neutron stars, *Nature Astron.* 8 (2024) 1020–1030. [arXiv:2404.05371](#), [doi:10.1038/s41550-024-02291-y](#).
- [94] D. Klahn, T. Blaschke, S. Typel, et al., Constraints on the high-density nuclear equation of state from the phenomenology of compact stars and heavy-ion collisions, *Phys. Rev. C* 74 (2006) 035802. [arXiv:nucl-th/0602038](#), [doi:10.1103/PhysRevC.74.035802](#).